Chinese Chemical Letters 34 (2023) 107966

Contents lists available at ScienceDirect

Chinese Chemical Letters

journal homepage: www.elsevier.com/locate/cclet

Treatment of Alzheimer's disease with small-molecule photosensitizers

Yefei Jiang[a], Zhiyong Zeng[a], Jianhua Yao[b,*], Ying Guan[b,*], Peipei Jia[a,c], Xiaoli Zhao[a], Lin Xu[a,c,**]

[a] Shanghai Key Laboratory of Green Chemistry and Chemical Processes, School of Chemistry and Molecular Engineering, East China Normal University, Shanghai 200062, China
[b] Joint Institute of Tobacco and Health, Yunnan Academy of Tobacco Science, Kunming 650024, China
[c] Wuhu Hospital Affiliated to East China Normal University (The Second People's Hospital of Wuhu), Wuhu 241001, China

ARTICLE INFO

Article history:
Received 5 July 2022
Revised 20 October 2022
Accepted 24 October 2022
Available online 1 November 2022

Keywords:
Alzheimer's disease
Photosensitizer
Aβ aggregation
PDT

ABSTRACT

Alzheimer's disease is a neurodegenerative disease that signals for excess β-amyloid (Aβ) aggregation. Although people have made great attempts to control the aggregation of Aβ, no effective medications have been produced yet. Due to its excellent temporal and spatial selectivity, photodynamic treatment has been gradually employed and interfered in the aggregation process of Aβ, with some achievement. To enhance the research and application of photodynamic therapy in Alzheimer's disease, this paper reviews the progress of small-molecule photosensitizers in the treatment of Alzheimer's disease in recent years and outlines existing tactics and potential obstacles.

1. Introduction

Alzheimer's disease (AD) is a progressive and neurodegenerative disease that leads to neuronal cell death and cognitive loss [1,2] and is the most common cause of age-related dementia, affecting more than 20 million people worldwide [3]. Previous compounds, such as donepezil, galantamine, rivastigmine, and memantine for the treatment of AD have limited effects [4]. In addition, they do not prevent neuronal loss, brain atrophy, and the progressive deterioration of cognition. So far, the cause of Alzheimer's disease remains unresolved. Glenner and Wong first isolated β-amyloid (Aβ) from the brains of AD patients in 1984 [5], and the "amyloid hypothesis" has garnered the attention and support of a growing number of scientists [6]. The hypothesis holds that the self-assembly of Aβ and the deposition of its aggregates are the main events in the pathogenesis of AD [7]. Although the amyloid hypothesis has arguably been supported over the past four decades by genetic, molecular, cell biological, biochemical, and transgenic studies, it remains controversial [8]. Owing to clearance failure or abnormal overproduction, the level of Aβ in the brain gradually increases, resulting in Aβ monomers self-assembling into toxic oligomers and fibre aggregates. The body is characterized by intracellular neurofibrillary tangles and progressive neuronal loss [9]. Early researchers believed that Aβ-related toxicity comes from mature amyloid plaques, while recent studies have shown that soluble oligomers formed in the early stage of aggregation can lead to greater neuronal damage [10]. Although the original function of Aβ and the mechanism of neurotoxicity induced by self-assembly have not been clarified, Aβ aggregates play a pathogenic role in AD pathology, which has been supported by a large amount of data and findings during the past decades [11,12]. Inhibiting Aβ aggregation or degrading aggregates [13] is considered to be an attractive therapeutic and preventive strategy for AD treatment [14]. Even though researchers have made tremendous efforts [15–17], they still face failure in clinics, mainly due to relatively low targeting, high toxicity and side effects [18,19].

PDT is a non-invasive treatment that refers to the reaction between photosensitizers and oxygen-containing substrates (such as oxygen and water) under specific wavelength light irradiation to generate $^1O_2$ or other reactive oxygen species (ROS, usually peroxides, free hydroxyl radicals, *etc.*) that can react with biological macromolecules to effectively kill the lesion site and achieve the purpose of treatment [20–25]. To date, PDT has been widely applied in various fields, such as tumour therapy and *in vivo* imaging [26–30]. Considering its targeted, safety, low toxicity and limited

* Corresponding authors.
** Corresponding author at: Shanghai Key Laboratory of Green Chemistry and Chemical Processes, School of Chemistry and Molecular Engineering, East China Normal University, Shanghai 200062, China.
E-mail addresses: jhyao_2007@126.com (J. Yao), 125176198@qq.com (Y. Guan), lxu@chem.ecnu.edu.cn (L. Xu).

https://doi.org/10.1016/j.cclet.2022.107966
1001-8417/

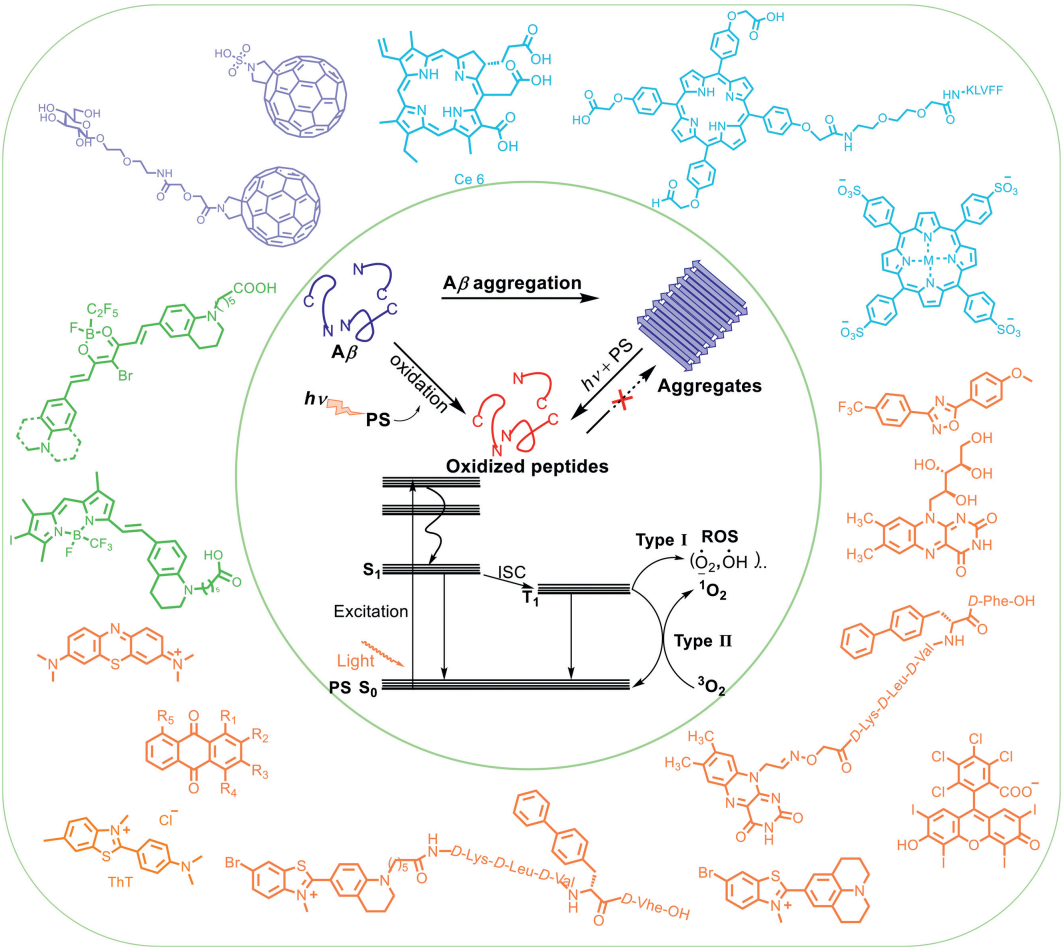

Fig. 1. Schematic diagram of small-molecule photosensitizers in the treatment of AD.

side effects, PDT has progressively become a significant method in clinical treatment [31–33]. For the past few years, the application of PDT in AD has attracted widespread attention [34,35]. The utilization of small-molecule photosensitizers not only has the benefits of controllable construction and simple adjustment but also causes less damage to the surrounding area during treatment than surgery or chemotherapy. Thus, PDT has extraordinary application potential in the treatment of AD. Recent studies have shown that light-assisted therapy can greatly improve Aβ aggregation-induced neurotoxicity, although it still has some challenges and difficulties in practical application.

This paper reviews some application examples of small-molecule photosensitizers in the treatment of AD (Fig. 1). These small-molecule photosensitizers are divided into four groups: (i) fullerene and its derivatives, (ii) porphyrin and its derivatives, (iii) N or O heterocyclic compounds, and (iv) fluoroboron compounds. Their PDT properties and possible mechanisms are introduced. Finally, certain issues and prospects of small-molecule photosensitizers in the treatment of AD are summarized to provide a reference for the design of a new generation of molecules.

2. Small-molecule photosensitizers

2.1. Fullerenes and its derivatives

Fullerene and their derivatives as photosensitizers have great potential in PDT treatment [36], due to its high electron affinity, high surface/volume ratio [37], and high yield of $^1O_2$ generation under UV light [38]. Therefore, some achievements have been made in inhibiting Aβ aggregation by fullerene derivatives.

In 2010, Toshima and co-workers reported the example of fullerene compounds degrading Aβ under light [39]. They designed and synthesized compounds **1** and **2** (Fig. 2a), in which the fullerene moiety showed high affinity for the 16–20 amino acid residue KLVFF in the central part of the Aβ42 peptide, and the IC_{50} values of **1** and **2** were 35 and 192 μmol/L, respectively. Therefore, they chose compound **1** to study its inhibition of Aβ42 aggregation. The results showed that compound **1** could prevent Aβ42 aggregation in a concentration-dependant manner even without light irradiation, and the inhibition ability was improved after light irradiation. More importantly, transmission electron microscope (TEM) confirmed that compound **1** could corrupt the Aβ42 monomer as well as its aggregate under UV irradiation. Figs. 2b and c clearly showed that in the presence of **1**, the generation of high-molecular-weight Aβ42 was efficiently inhibited. Electron paramagnetic resonance (EPR) analysis indicated that the degradation of Aβ42 monomers and oligomers was attributed to the reactive oxygen species (ROS) produced by fullerenes and photoexcited O_2.

To improve its biological solubility, Toshima and co-workers introduced water-soluble units into fullerenes to obtain compounds **3** and **4** (Fig. 2d) [40]. These compounds could also degrade Aβ under light. The binding abilities of **3** and **4** with Aβ42 were examined by observing the inhibitory effect using a thioflavin T (ThT) fluorescence assay, which showed that **3** had a higher affinity for Aβ than **4**. Based on this, compound **3** was selected for further study, and the inhibitory concentration (IC_{50}) value of compound **3** with photoirradiation was 5.9 times higher than that of without

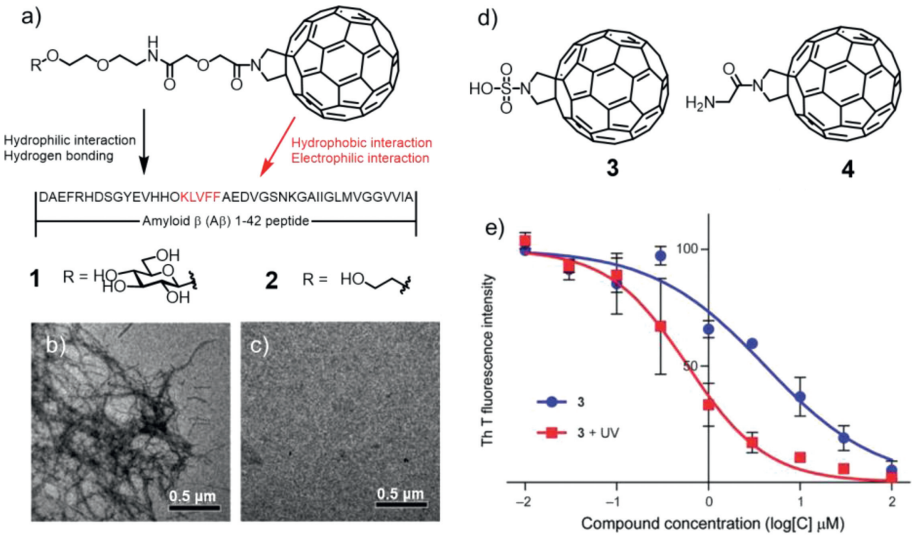

Fig. 2. (a) Chemical structures of fullerene photosensitizers **1** and **2**. (b) Before and (c) after illumination TEM analysis of the prevention of Aβ42 fibril formation by 1. Reproduced with permission [39]. Copyright 2010, The Royal Society of Chemistry. (d) Chemical structures of fullerene photosensitizers **3** and **4**. (e) Schematic diagram of the combination curve of ThT to Aβ42 fibrils with (red line) and without (blue line) photoirradiation in the presence of **3**. Reproduced with permission [40]. Copyright 2011, Wiley-VCH Verlag GmbH&Co. KGaA, Weinheim.

photoirradiation, indicating that the Aβ42 aggregation inhibitory ability of **3** was higher under light illumination than without photoirradiation (Fig. 2e). Further cell experiments showed that compound **3** could greatly control Aβ mediated cytotoxicity. Under light conditions, the survival rate of rat phaeochromocytoma (PC12) cells containing Aβ was greatly improved by the presence of compound **3**. The authors used fullerene-sugar hybrid degrading Aβ42 monomer and oligomers under photo-irradiation, developing a novel method for potential treatment in AD.

2.2. Porphyrin and its derivatives

Porphyrin and its derivatives as common photosensitizers have the following advantages: relatively high $^1O_2$ quantum yields and low energy Q-bands, making them widely studied in PDT and cancer imaging [41].

Based on this, porphyrin was reported to regulate the formation of Aβ40 fibers [42]. In 2014, porphyrin and its derivatives were used to study the photodegradation of Aβ by Toshima and coworkers [43]. They prepared compound **5** and polypeptide derivatives compound **6** (Fig. 3a), which could inhibit the aggregation of Aβ as well. Next, the binding abilities of **5** and **6** with Aβ42 were also examined by observing the inhibitory effect using the ThT assay. The IC_{50} value could be attained by the plots of Figs. 3b and c, which showed that the IC_{50} values of **5** and **6** were 11.0 and 3.56 μmol/L, indicating that both **5** and **6** had high affinities for Aβ42. Then, a ThT assay was used to confirm the difference in Aβ42 aggregation-inhibitory abilities of **5** and **6** with and without photoirradiation. These results verified that **5** and **6** inhibited Aβ42 aggregation with higher efficiency under light conditions than without photoirradiation. It is noteworthy that the inhibitory ability of **6** was 45 times higher than that of compound **3**, and it could not only oxidize Aβ monomers but also corrupt their oligomers under photoirradiation. In addition, compound **6** could crucially inhibit Aβ42-mediated PC12 cytotoxicity, and the inhibitory ability of compound **6** was 30 times that of compound **1**.

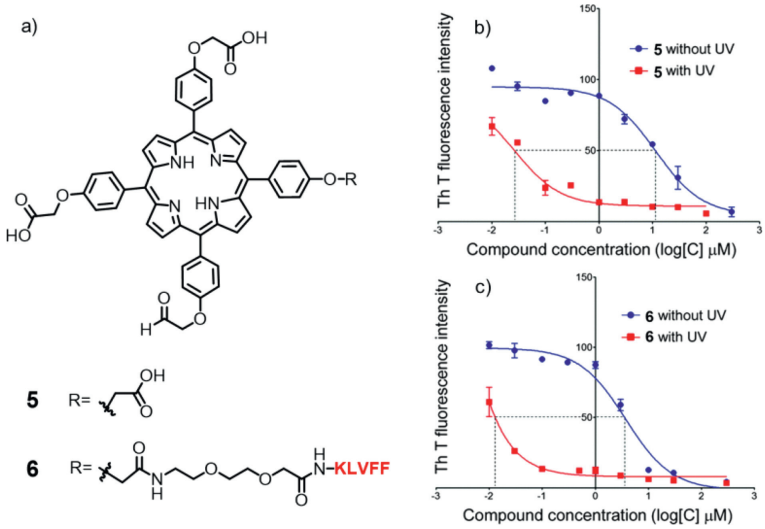

Fig. 3. (a) Chemical structure of porphyrin derivatives **5** and **6**. (b, c) Schematic diagram of the combination curve of ThT to Aβ42 fibrils with (red line) and without (blue line) photoirradiation in the presence of **5** and **6**. Reproduced with permission [43]. Copyright 2014, The Royal Society of Chemistry.

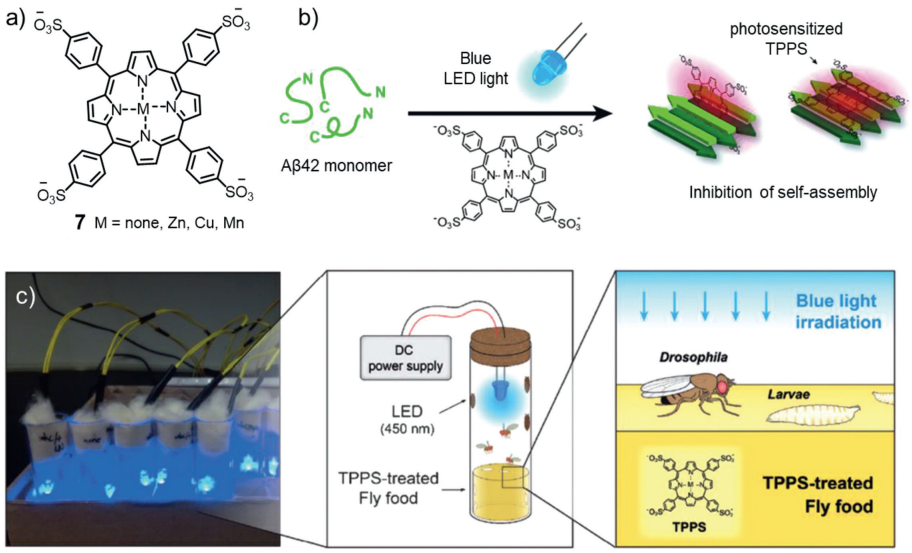

Fig. 4. (a) Structure of photosensitizer **7**. (b) Schematic diagram of compound **7** inhibiting Aβ protein self-assembly into fibers under light. (c) Blue LED light field exposure device. Blue LED photosensitive TPPS is mixed with *Drosophila* food (right). Reproduced with permission [44]. Copyright 2015, Wiley-VCH Verlag GmbH&Co. KGaA, Weinheim.

On this basis, *meso*–tetra(4-sulfonatophenyl)porphyrin (TPPS, compound **7**) was prepared by Park and co-workers (Fig. 4a) [44]. Through a variety of photochemical analyses (including circular dichroism, atomic force microscopy, dot plot, and native gel electrophoresis), they proved that photosensitizer **7** could regulate Aβ self-assembly into fibrils under blue LED light by generating reactive oxygen species (ROS). In addition, the changes in the optical properties of the metal in the centre of the porphyrin ring also have different effects on the photoinhibition and toxicity of Aβ aggregation. Moreover, the Drosophila *in vivo* model experiment showed that under blue light irradiation (Fig. 4b), a variety of neurodegenerative manifestations (such as locomotion defects, lifespan reduction, vacuolization of the brain, and neuromuscular junction morphology defects) caused by Aβ overexpression resulted in different degrees of remission (Fig. 4c). It was verified that compound **7** could inhibit Aβ aggregation *in vitro* and restore Aβ-induced nerve injury, showing that porphyrin and its derivatives had high potential as phototherapeutic agents for the treatment of AD.

Unlike porphyrins with 22 π electrons and 4 pyrroles, chlorin e6 (Ce6, compound **8**, Fig. 5a) has only 20 π electrons and 3 pyrroles on the core. Given its minimum dark toxicity, high stability, great solubility, and large singlet oxygen production quantum yield, Rahimipour and co-workers found that Ce6 could bind Aβ_{40} with high affinity and selectivity, dramatically enhancing its ability to restrain Aβ aggregation and toxicity under light conditions [45]. The mechanism studies showed that it was mediated through type II photo-oxidation involving singlet oxygen. TEM was applied to validate the strong anti-amyloidogenic activity of Ce6 under photoirradiation (Figs. 5b-d) using the Aβ samples from the ThT assay. It was fortunate to find that ageing of monomeric Aβ (20 μmol/L) and in the presence of Ce6 (2 μmol/L) both formed well-defined fibrils under dark conditions. Conversely, under photoaging, the mixture of Aβ and Ce6 generated aggregates with different morphologies, and the lengths of the aggregates were obviously shorter. In the dark, Ce6 could also reverse the aggregation process of amyloid protein by binding its soluble oligomer. HSQC NMR spectroscopy, ThT assay, amino acid analysis, SDS/PAGE, and EPR spectroscopy were used to prove that the photocatalytic amount of Ce6 was capable of destroying Aβ histidine residues (H6, H13, H14) and inducing Aβ crosslinking by producing $^1O_2$.

Next, the author tested whether Ce6 could modulate the binding ability between Cu^{2+} and Aβ and reduce Cu^{2+}-induced aggregation and toxicity. The ThT fluorescence control experiment showed that the presence of Cu^{2+} (0.3 equiv.) accelerated the aggregation process of Aβ, indicating that Cu^{2+} could promote the formation of the ThT-active β-sheet structure (Fig. 5e). However, with the addition of Ce6 (0.025 equiv.), the lag phase was extended to approximately 22 h and reduced its aggregation, validating that Ce6 has a higher binding ability with Aβ His-residues than Cu^{2+} in the early Aβ aggregation process. Next, PC12 cells were used to evaluate the protective effect of Ce6 against Cu^{2+}-induced Aβ toxicity (Fig. 5f). Under the conditions tested, the presence of Cu^{2+} increased the toxicity of Aβ. In addition, Cu^{2+} alone had no toxic effect on cells, which was consistent with the ThT assay, suggesting that Ce6 could revert the effects of Cu^{2+}. This study demonstrated the great potential of Ce6 as a multifunctional drug for the treatment of AD and showed that three N-terminal Aβ histidine residues were suitable target for specific drugs.

2.3. N or O heterocyclic compounds

N or O heterocyclic compounds such as ThT, riboflavin (vitamin B2), rose bengal (RB), methylene blue (MB) and some other photosensitizers have been extensively studied in antibacterial and AD photodynamic therapy, with high triplet quantum yields and low side effects of phototoxicity [46].

In 2009, to study the mechanism of how amyloid fibrils form, Goto's group combined the fluorescent dye ThT (compound **9**, Fig. 6a) with total internal fluorescence microscopy (TIRFM) [47]. It was successful to gain information about the morphology, growth rate, and extension direction at the single fibre level in real time. It was also found that under 442 nm wavelength light irradiation, ThT could generate $^1O_2$ after being excited and then inhibit β2-microglobulin (β2-m) growth or destroy K3 fibrils, in which β2-m was a classic immunoglobulin domain composed of 99 amino acid residues and seven β-stands [48]. Fig. 6b showed the real-time observation of the growth of β2-m and K3 fibrils. Fluorescent spots of seeds were observed as soon as the growth was initiated, and the growth of β2-m fibrils was also observed. With time, the extension of β2-m fibrils stopped. The author assumed that the growth was inhibited by laser irradiation over time, indicating that the growth of β2-m fibrils counted on the laser beam and its intensity to a great extent. Next, K3 fibril growth at neutral pH was observed, and the laser power and the duration were the

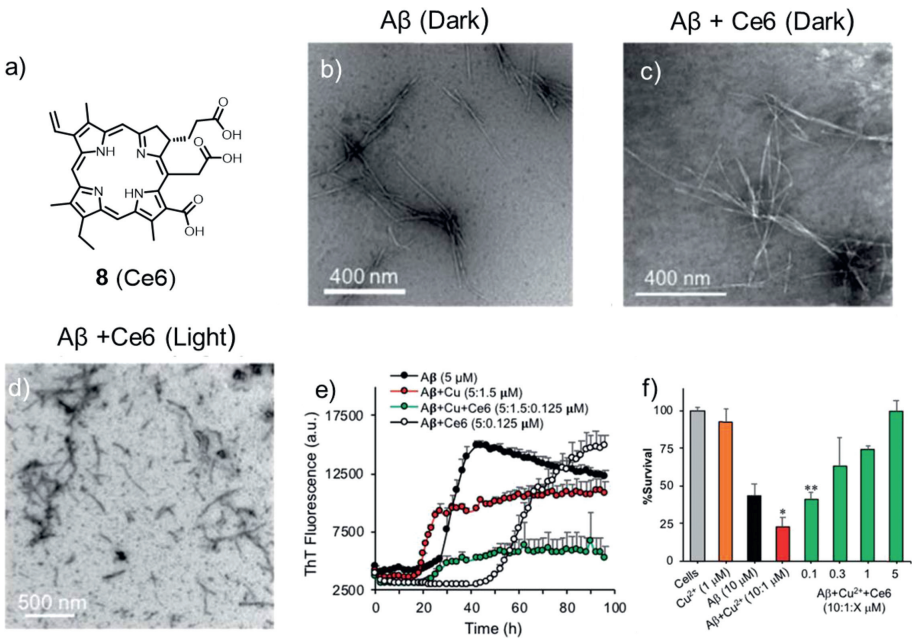

Fig. 5. (a) Chemical structure of photosensitizer **8**. (b-d) TEM images of Aβ influenced by Ce6. TEM image of Aβ incubated in the absence or presence of Ce6 in darkness or after 1 h photoirradiation following 72 h of incubation in darkness. (e, f) Effects of Ce6 on Aβ aggregation and toxicity induced by Cu^{2+}. Reproduced with permission [45]. Copyright 2019, The Royal Society of Chemistry.

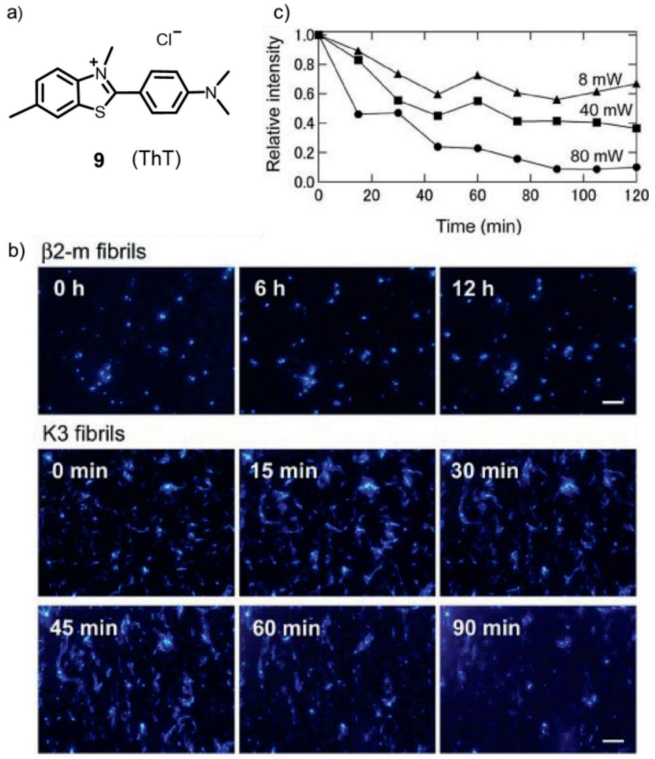

Fig. 6. (a) Chemical structure of photosensitizer **9**. (b) Growth process of β2-m and K3 fibers in the presence of ThT. (c) Relationship between fibre damage and laser power. Copied with permission [47]. Copyright 2009, Elsevier.

same as above. At time 0, several K3 fibrils already occurred at many sites, which implied that the short fibrils had already generated in the sample when K3 peptides were dissolved. Although K3 fibrils grew for some time, reaching lengths of several micrometres (see image at 15 min), the growth stopped at 30 min. In addition, with increasing duration, the extended fibrils disappeared (images from 45 min to 90 min). This unexpected phenomenon may be due to the laser beam causing the inhibition of fibril growth and decomposition of the performed fibrils. To take the dependence of laser power on destruction into account, the laser power was varied between 8 and 80 milliwatts (Fig. 6c). As the laser power increased, the destruction speed was faster and the range was wider, demonstrating that the disappearance of K3 fibrils was induced by the laser beam irradiation of ThT bound to fibrils. These results indicated that the light-induced decomposition of amyloid fibrils combined with an amyloid-specific dye in the treatment or prevention of dialysis-related amyloidosis has a promising future.

In 2014, Kanai and co-workers selected vitamin B2 (compound **10**, Fig. 7a) to catalyse the photooxygenation of Aβ [49], owing to its potential advantages: (1) corrosion resistance of aqueous media with molecular oxygen as the sole oxidant [50]; (2) low toxicity of riboflavin as an organocatalyst; (3) possibility of on/off control with harmless visible light. In order to test the oxidation capacity of the riboflavin catalyst to Aβ under visible light irradiation, a phosphate buffer solution (pH 7.4) containing Aβ1–42 and riboflavin was irradiated using a fluorescent lamp at 37 °C, and the reaction was monitored by MALDI-TOF MS (Fig. 7b), proving that riboflavin could catalyse the oxidation of one or more of the three amino acid residues (Tyr, His, Met) of Aβ under visible light. In addition, the ThT assay illustrated that the fluorescence intensity of oxygenated Aβ was much lower than that of native Aβ, indicating that oxygenated Aβ did not construct cross β-sheet aggregates (Fig. 7c). The fluorescence intensity of cross β-sheet aggregates increases with increased amyloid aggregation (generating a cross β-sheet) [51]. The aggregation ability of oligomer/protofibril Aβ to fibrils was almost completely inhibited after oxygenation, and the neurotoxicity of oxygenated Aβ was much lower than that of natural Aβ. To improve the selective oxidation of the photosensitizer, riboflavin was modified to target peptides to obtain compound **11**. The cell viability test showed that compound **11** greatly reduced Aβ toxicity and improved cell survival after photooxidation (Fig. 7d). In addition, co-treatment with oxygenated antibodies could significantly inhibit the aggregation ability and cytotoxicity of natural Aβ.

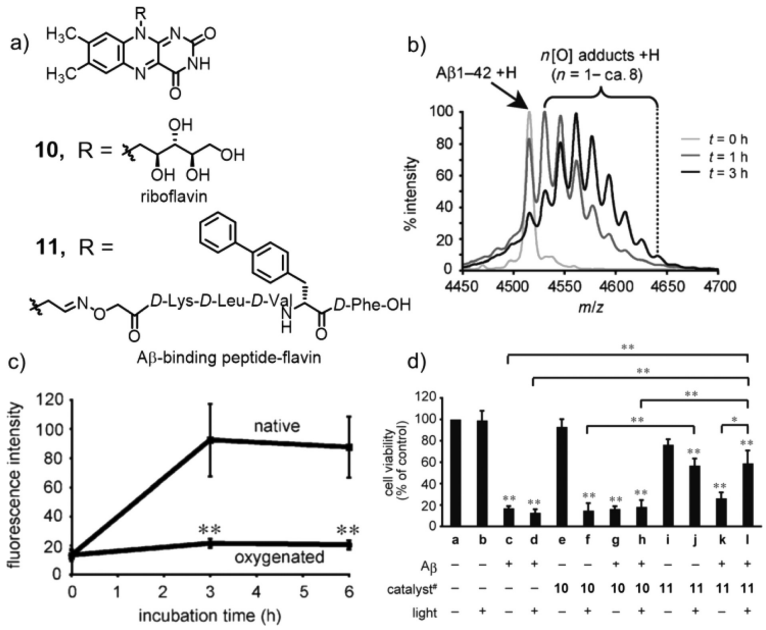

Fig. 7. (a) Chemical structures of riboflavin **10** and its derivative **11**. (b) MALDI-TOF mass spectra of the reaction mixture at different times after illumination. (c) ThT fluorescence assay. (d) Photooxygenation in the presence of PC12 cells. Reproduced with permission [49]. Copyright 2014, Wiley-VCH Verlag GmbH&Co. KGaA, Weinheim.

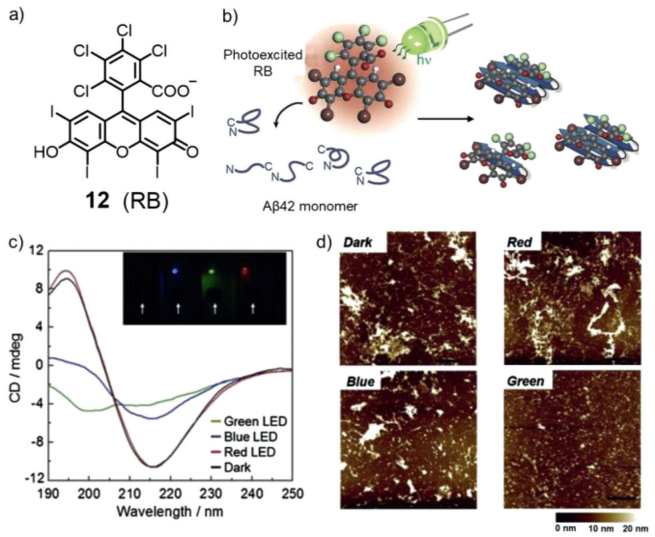

Fig. 8. (a) Chemical structure of photosensitizer **12**. (b) Schematic diagram of photoexcited RB inhibiting Aβ aggregation. (c) CD spectra (insert: image of red, green, and blue LEDs). (d) AFM images of Aβ42 solutions in the presence of RB under LED illumination. Reproduced with permission [52]. Copyright 2014, Elsevier.

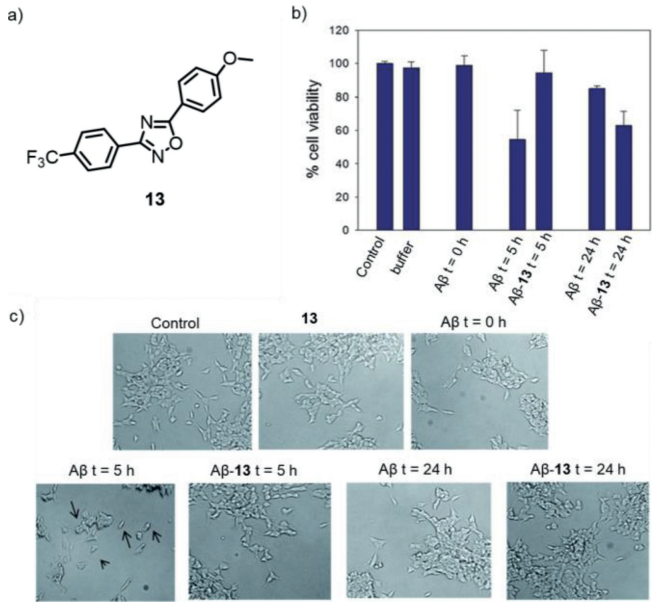

Fig. 9. (a) Chemical structure of photosensitizer **13**. (b) The viability of LAN5 cells at different times with or without **13**. (c) Microscopic images for the same samples. Reproduced with permission [53]. Copyright 2015, The Royal Society of Chemistry.

In 2015, by screening a variety of dyes, Park and co-workers identified RB (compound **12**, Fig. 8a), which showed a remarkable redshift and an intense enhancement of fluorescence emission in the presence of Aβ42, showing strong affinity to Aβ42. They reported visible light-induced inhibition of Aβ42 aggregation by photosensitizing RB (Fig. 8b) [52]. It might be due to that a ground state RB was boosted into a high energy state by absorption of visible light, generating $^1O_2$ by energy transfer to O_2, and modulating Aβ aggregation. Through circular dichroism (CD) analysis (Fig. 8c), light spectrum and AFM (Fig. 8d) analysis, it was believed that green light photoexcited RB regulates Aβ42 aggregation much more strongly than RB under dark conditions and other light. Moreover, RB could not only disturb the early steps of the Aβ42 self-assembly pathway but also inhibit the conformational transformation of the Aβ42 monomer and small aggregates to the β-sheet-rich structure under green LED irradiation. *In vitro* cell experiments also showed that light-stimulated RB effectively inhibited Aβ42 aggregation and reduced Aβ42-induced cytotoxicity.

In the same year, Biagio's group reported a new photosensitizer, 1,2,4-oxadiazoles (compound **13**, Fig. 9a), to interfere with Aβ self-assembly [53]. Light stimulation of compound **13** induced the formation of reaction intermediates and then reversed the accumulation of Aβ1–40 amino acids through photoinduced electron transfer (PET) or energy transfer (ET) mechanisms. In contrast to previous reports, Aβ was not oxidized but reacted with a photosensitizer to form an active species and then crosslinks with another molecule Aβ to form a non-toxic dimer and further form an

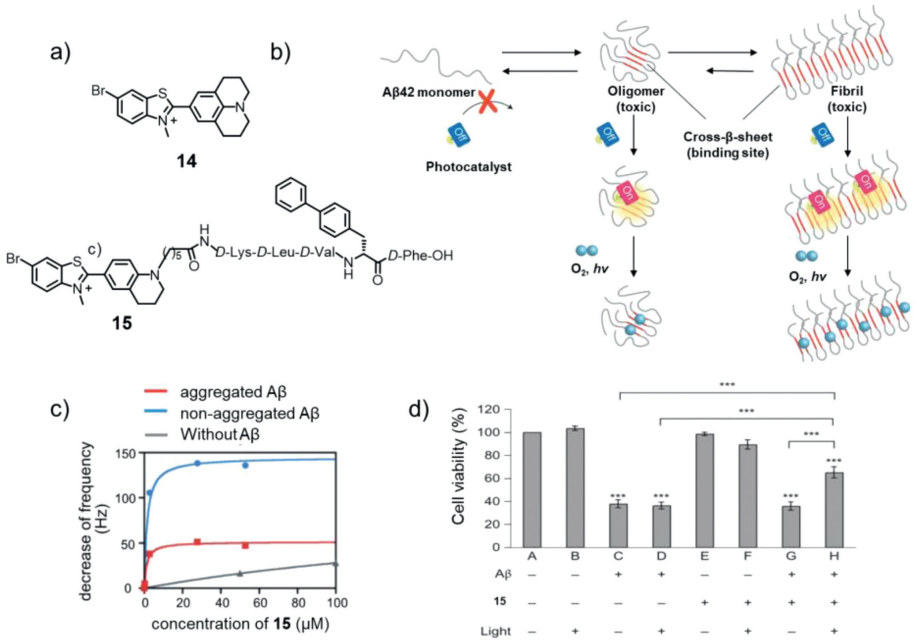

Fig. 10. (a) Chemical structures of the TaSCAc photosensitizers **14** and **15**. (b) Schematic diagram of treating AD with TaSCAc photosensitizer when the catalysts combine with cross-β-sheet structure, the catalyst is selectively activated to photooxidize the aggregates. (c) Binding affinity of **15** with nonaggregated/aggregated Aβ1–42 validated by quartz crystal microbalance. (d) Cell viability assay. A cell-culture medium (CM) that contained Aβ (20 μmol/L) and 15 (10 μmol/L) was photoirradiated ($\lambda = 500$ nm) for 30 min at 37 °C in PC12 cell-seeded wells, doubly diluted with CM (final Aβ species, 10 μmol/L), incubated at 37 °C under 5% CO_2 for 48 h and analysed for cell viability. Reproduced with permission [54]. Copyright 2016, Nature Publishing Group.

oligomer. An *in vitro* cytotoxicity assay was conducted to study the cytotoxicity of compound **13** and its possible influence on the formation of neurotoxic Aβ1–40, and the MTS assay was performed on the LNA5 neuroblastoma cell line. As shown in Fig. 9b, the main toxicity was due to the sample of Aβ1–40 alone incubated for 5 h, which may only contain oligomeric species. In the presence of photo-stimulated compound **13** for 5 h, no toxic effect was observed. After photo-stimulation for 24 h, the cell viability was reduced, indicating that compound **13** was able to inhibit Aβ aggregation under proper photoirradiation. Microscope images for the same sample were shown in Fig. 9c, which was consistent with the cell viability results. It is worth mentioning that this photosensitive conversion of Aβ into non-toxic oligomers may be an attractive strategy for the treatment of AD.

In 2016, Kanai and co-workers reported the target state-dependant photooxygenation catalyst **14** (Fig. 10a), which could be active only when bound to the characteristic cross-β-sheet structure of aggregated Aβ [54]. This unique activation method was also called the target-sensing catalyst activation (TaSCAc) method, which could greatly inhibit the occurrence of off-target reactions and significantly enhance the target selectivity of chemical modifications of the native protein. Fig. 10b illustrated the utilization of the TaSCAc protocol to design an on/off switchable photooxygention catalyst. When the catalyst was combined with the cross-β-sheet structures of aggregated amyloid proteins, the photooxygention catalyst could be selectively activated and photooxygenated the Aβ aggregates. When compound **14** was excited by light irradiation in the natural state, due to the electron-donor julolidine and the electron-acceptor bromo–substituted benzothiazole, the relaxation process was carried out through twisted intramolecular charge transfer (ICT), resulting in no fluorescence emission.

However, when **14** was combined with the cross-β-sheet structure, the axial bond rotation between the donor and receptor was hindered, interfering with the twisted ICT; thus, fluorescence was produced successfully during relaxation. In addition, excited electrons could also transform from S_1 to T_1 to produce $^1O_2$. To investigate the effects of Aβ photooxygenation in the presence of living cells, due to the toxicity of compound **14** to PC12 cells, a new catalyst **15** was designed, which has no toxicity to PC12 at concentrations up to 30 μmol/L. Although catalyst **15** could combine with aggregated and non-aggregated Aβ1–42 (Fig. 10c), the catalyst activity of **15** was activated only when binding with the cross-β-sheet structures of aggregated Aβ. As Fig. 10d illustrated, the cell viability under photoirradiation was higher than that without light illumination, which indicated that photooxygenation of Aβ catalysed by **15** in the presence of the cells weakened the toxicity of native Aβ. When **15** was combined with Aβ, under light conditions, the oxygenation reaction occured on His13, His14, and/or Met35 residues, resulting in the production of non-toxic oxygenated Aβ. It is noteworthy that **15** only reacted with the Aβ aggregate cross-β-sheet structure but did not react with other peptides.After oxygenation, the high-order structure of the protein was maintained without affecting its physiological function. This TaSCAc concept may inject new impetus into the design of therapeutic photooxygenation catalysts for selective removal of abnormal amyloid. The drawback of this method was that its excitation wavelength was only 500 nm, which might limit its application to a certain extent.

One of the remarkable advantages of MB (compound **16**, Fig. 11) as a drug for the light-induced treatment of neurodegenerative diseases is that it can cross the blood-brain barrier (BBB) [55]. Moreover, MB can be excited by the absorption of red light (>630 nm). Park's group discovered that under light conditions, MB monomers produce $^1O_2$ *via* the type II photochemical pathway, in which the energy from triplet state MB is transferred to molecular oxygen [56] and generated $^1O_2$, inhibiting Aβ aggregation and dissociating pre-existing aggregates. In addition, *Drosophila* AD model was used to study the *in vivo* efficacy of photosensitized inhibition of Aβ42 aggregation by MB. Under dark conditions, in the presence of MB, or under light irradiation without MB, the recovery of AD model was negligible. While, under light illumination, MB induced significantly recovery of locomotion defects and sup-

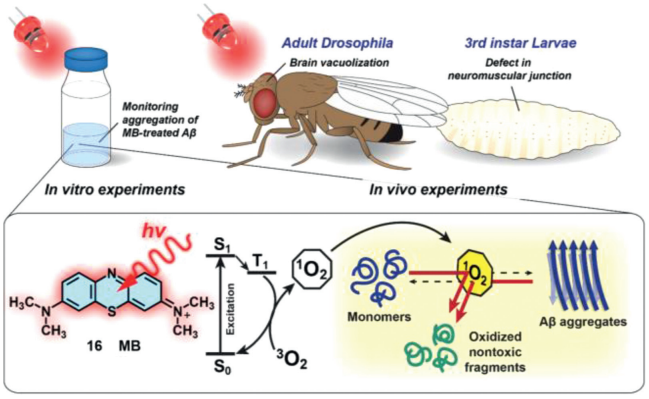

Fig. 11. Schematic of *in vivo* and *in vitro* Drosophila AD models to study the therapeutic effect of photosensitizer **16** on protein misfolding disease. Reproduced with permission [55]. Copyright 2017, Nature Publishing Group.

pressed Aβ42-induced toxicity in the *Drosophila* AD model, and *in vitro* experiments likewise showed that light-stimulated MB also had a superb effect on inhibiting neural performance (Fig. 11). MB has been studied as a therapeutic chemical for more than a century and is expected to be followed by more research into AD treatment.

Anthraquinone (AQ)-based dyes have already been widely applied to photovoltaics [57], photocatalysts [58], photoactive peptides [59], and cell imaging [60]. Therefore, Lim's group [61] selected and modified a series of derivatives from **9,10-AQ** to test effective photosensitizers that could oxidatively modify Aβ peptides and inhibit their aggregation. The AQ derivatives were normally divided into two groups (Fig. 12a): group A (**HQ**, **Ali**, **Qui** and **Pur**) contains a hydroxyl group on the R_1 position forming a *quasi*-ring with adjacent ketone and additional hydroxyl groups on R_2 and R_4, or both; group B (**Dan**, **Rhe** and **Alo**) possesses hydroxyl groups on both R_1 and R_5 forming two *quasi*-rings and structure variance on R_3. A previous report showed that AQ would generate singlet oxygen ($^1O_2$) under photoactivation; thus, it was anticipated that AQ derivatives could oxidize amino acid residues in Aβ and regulate Aβ aggregation (Fig. 12b). DFT calculations were conducted to study the mechanism for $^1O_2$ generation, indicating that hydroxyanthraquinone showed excited-state intramolecular hydrogen transfer (ESIHT) from hydroxyl groups to the adjacent ketone functional group in the process of photoactivation. Moreover, the DFT calculation also verified the significance of the position of the hydroxyl group to adjust the energy gap between S_1 and T_1, which affected its ability to produce $^1O_2$. Under light conditions, AQ produced $^1O_2$ and oxidizes His13, His14, and Met35 residues to varying degrees, substantiated by the MS studies. Inhibition experiments were also conducted employing Aβ42, and it was fortunate to find that the addition of AQ derivatives could inhibit the aggregation of Aβ42.

Owing to the excellent properties of AQ derivatives, their biological efficacies were worth studying. It was proven that AQ

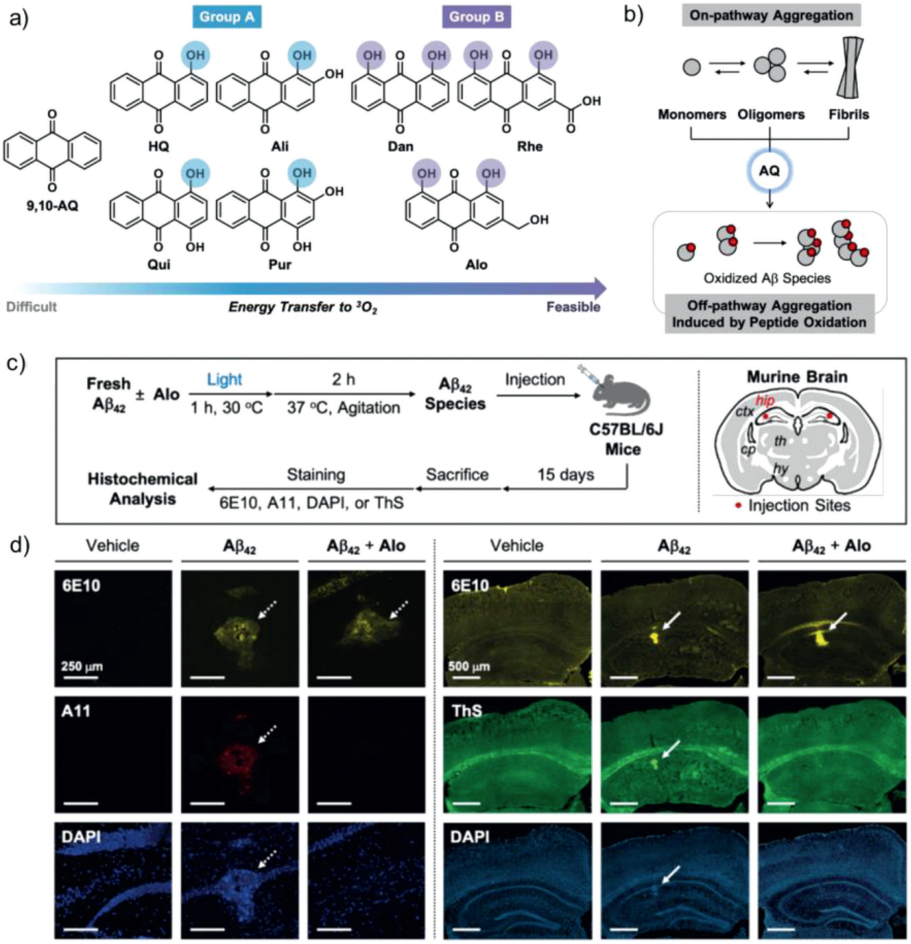

Fig. 12. (a) Chemical structures of the AQ molecules. (b) Schematic diagram of the light-activated AQ series regulator Aβ aggregation path. (c) Schematic description of histochemical studies and injection sites in the brain. (d) Microscopic images of the hippocampi of C57BL/6J mice injected with vehicle, Aβ42, or Alo-treated Aβ42. Copied with permission [61]. Copyright 2021, ChemRxiv.

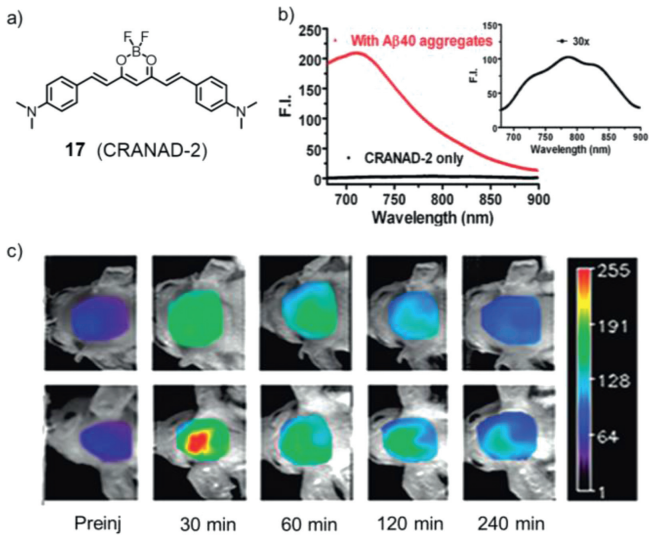

Fig. 13. (a) Chemical structure of photosensitizer **17**. (b) Fluorescence of CRANAD-2 (100 nmol/L) induced by Aβ aggregates (red line). CRANAD-2 alone (black line). (c) Representative images of Tg2576 mice and control littermates at different time points before and after iv injection of 5.0 mg/kg CRANAD-2. Reproduced with permission [64]. Copyright 2009, American Chemical Society.

has an excellent ability to cross the blood-brain barrier (BBB, which was a critical factor for chemical reagents to be applied in the brain [62]. Because of the limited solubility of **9,10-AQ** in-water, **Alo** was selected to examine the histochemical investigations *in vivo*. As illustrated in Fig. 12c, after the injection of **Alo** for 15 days, brain sections were obtained. Fig. 12d showed that the brain sample injected with Aβ42 species oxidized by photoactivated **Alo** showed negligible oligomeric and fibrillar aggregates. Overall, the experimental and computational research illuminates that through the hydrogen bond modulation of ESIHT-based photosensitizers, it successfully inhibited Aβ aggregation and possessed bright prospects in AD treatment.

2.4. Fluoroboron compounds

Fluoroboron (bodipy), as a typical fluorescent dye, has the following characteristics: low dark toxicities, high extinction coefficients, and low photobleaching quantum yields [63]. The addition of heavy halogen atoms to pyrrole ring increases the triplet yield [46] and improve PDT performance as photosensitizer molecules.

In 2009, Moore's group designed a new compound, fluoroboron CRANAD-2 (compound **17**, Fig. 13a), and reported its application *in vivo* imaging [64]. With the ideal emission length ($\lambda_{max(em)} = 760$ nm in methanol) of CRANAD-2, an *in vitro* test was conducted. When compound **17** entered the brain and combined with Aβ40, the fluorescence intensity greatly increased up to 70-fold and showed a 90 nm blueshift and a large increase in quantum yield (Fig. 13b), displaying a "turn on" phenomenon. Through blood-brain barrier penetrating test, CRANAD-2 showed great BBB penetrating ability. Next, to prove the feasibility of compound **17** as an NIR imaging probe, transgenic 19-month-old Tg2576 mice carrying transgenic Aβ were used, and wild-type littermates were used as controls. As Fig. 13c showed, after injection of compound **17**, plaques were observed in the brains of transgenic mice. However, there were no plaques found in wild-type littermates. These results indicated that compound **17**, as an NIR probe, could label senile plaques, especially *in vivo*.

Based on previous research on CRANAD-2, Kanai's group designed and synthesized a series of fluoroboron compounds as photoactivatable oxygenation catalysts of Aβ (Fig. 14a) [65]. A bromine was introduced to CRANAD-2 to enhance the generation of singlet oxygen ($^1O_2$), allowing for Aβ oxygenation. Then, julolidine and perfluoroalkyl borate fragments were used as electron donor and acceptor components, respectively, to fulfil excitation with longer wavelength light. Moreover, a carboxyl group was introduced to improve the solubility. Amongst all catalysts, compound **18** exhibited the highest photooxygenation of Aβ aggregates under 780-nm

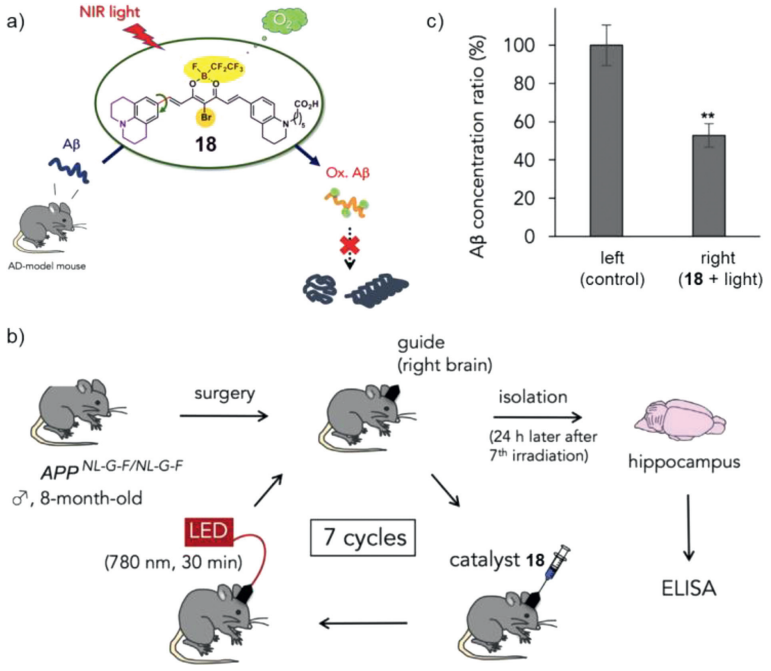

Fig. 14. (a) Schematic diagram of photosensitizer **18** in the treatment of AD. (b, c) Catalytic photooxygenation of Aβ by catalyst **18** in the living brain of an AD-model mouse. Reproduced with permission [65]. Copyright 2018, Elesevier.

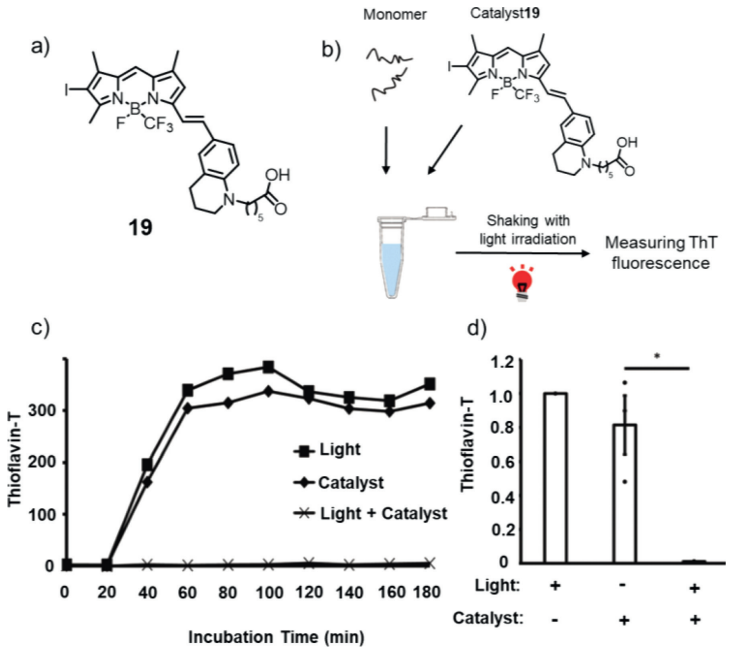

Fig. 15. (a) Chemical structure of photosensitizer **19**. (b) Experimental scheme of the *in vitro* fibril formation assay. (c) The sequential transition of tau fibrils measured by ThT fluorescence. (d) The amount of tau fibrils at 3 h of incubation measured by ThT fluorescence. Reproduced with permission [66]. Copyright 2019, The Royal Society of Chemistry.

light irradiation. Next, viscosity dependence experiments, DFT calculations, MALDI-TOF MS, and other experiments were conducted to demonstrate that catalyst **18** furnished a cross-β-sheet-sensing activation property and exhibited high selectivity towards aggregated Aβ. To examine the biocompatibility of catalyst **18**, *in vivo* experiments on mice were carried out. Fig. 14b showed that after injection of catalyst **18** into the right hippocampus and irradiation with 780-nm light for 30 min, this procedure was repeated seven times over 7 days. As a result, with photooxygenation, the concentration of Aβ1–42 in the right hippocampus was apparently lower (47% reduction, Fig. 14c) than that on the left side. Consequently, catalyst **18** could induce photooxygenation in the hippocampus of living mice, reducing Aβ1–42 levels in the brain. Notably, the bioavailability of PDT was greatly improved compared with that in previous work.

In addition to Aβ, the severity and distribution of neurofibrillary tangles formed by tau amyloid are known to be associated with decreased cognitive ability. However, the oxidation activity of compound **18** to tau protein was relatively low, as demonstrated by the photooxygenation experiment. Therefore, catalyst **19** (Fig. 15a) was designed to effectively photo oxidize tau amyloid [66]. Through structural modifications, the maximum absorption wavelength of **19** could reach 652 nm. First, the photooxidation of tau protein by catalyst **19** was studied using the wild type recombinant tau repeat domain (RDWT). MALDI-TOF-MS and HPLC were conducted to prove that photocatalyst **19** was on/off switchable by binding/nonbinding to aggregated tau amyloid. Next, to analyse the influence of tau photooxidation on its aggregation process, ThT was utilized in measuring aggregation properties (Fig. 15b), in which the ThT fluorescence intensity illustrated the amount of cross-β-sheet. As shown in Figs. 15c and d, the ThT fluorescence intensity of recombinant photo-oxygenated RDWT utilizing **19** (light + catalyst) was prominently lower than that of the native RDWT (light or catalyst), indicating that there were no fibrils generated by the photo-oxygenated tau RDWT. Both *in vivo* and *in vitro* experiments showed that the photooxidation of the catalyst substantially reduced the propagation activity of tau, resulting in the inhibition of the formation of tau amyloid *in vitro* [67].

3. Summary and prospects

The assembly of Aβ peptides into cross-β-sheet aggregates is a critical hallmark of AD [68–72]. However, the exact mechanism by which this aggregation leads to a decline in brain function has not yet been exemplified. Through tremendous efforts scientists have made over the past decade, inhibiting Aβ aggregation may be an essential and effective approach for the treatment of AD. Due to its high spatiotemporal selectivity and minimal invasiveness, PDT is an excellent candidate for use as a component in the exploration stage of AD. As shown in Table 1, this paper reviews the research progress of PDT small-molecule photosensitizers in the treatment of AD, including three types of photosensitizers, their corresponding excitation wavelengths, and targeted Aβ peptides.

With research progress, researchers have developed highly selective, infrared-absorbing, and non-toxic small-molecule photosensitizers. The photosensitizers also evolved from the cellular study to the mouse experiment and from non-targeted therapy to targeted therapy, which laid a solid foundation for the further study of PDT treatment of AD. However, the relatively complex physiological environment of the human body is a challenge for the application of small-molecule photosensitizers at the clinical level, which has limited the ability of researchers to obtain these results. Since Aβ aggregates in AD patients exist in the deep brain, the content of human amyloid may be much lower than that in AD model mice. To tackle these realistic problems, first, the design of photosensitizers with lower toxicity and better efficacy would be helpful [73–75]. Second, in-depth research on amyloid in the human brain is also needed. Fortunately, through more than a decade of research, PDT treatment of AD has gradually become a promising field despite many challenges. The study of photosensitive inhibition of Aβ self-assembly is still in its infancy, and we are convinced that PDT treatment of AD will be realized in the near future.

Table 1
Research status of small molecule photosensitizers in the treatment of AD.

Photo-sensitizer	Year of publication	Excitation wavelength (nm)	Target	Biological model	Comments	Refs.
ThT	2009	442	Aβ40	–	Degradation of fibre under light	[47]
Fullerene	2010	365	Aβ42	–	Inhibit Aβ monomer/oligomer aggregation	[39]
Fullerene	2010	365	Aβ42	PC12	Inhibition of Aβ42 mediated cytotoxicity	[40]
Riboflavin T	2013	White	Aβ42	PC12	Tyr10, His13, His14 and Met35 are oxygenated	[49]
Porphyrin	2014	365	Aβ42	PC12	Aβ42 was degraded under light irradiation to inhibit cytotoxicity	[43]
TPPS	2015	450	Aβ42	Drosophila	A variety of neurodegenerative manifestations in AD Drosophila model were inhibited	[44]
Rose bengal	2015	525	Aβ42	PC12	Inhibit the transformation of Aβ monomer to β-sheet-rich structures	[52]
1,2,4-Oxadiazole	2015	260	Aβ40	LAN5	Interacts with Aβ monomer to form non-toxic aggregate	[53]
ThT derivative	2016	500	Aβ42	PC12	Target sensing catalyst activation, only combined with cross β-structure is active	[54]
MB	2017	630	Aβ42	Drosophila	The excited MB has de-composition Aβ42 aggregates to reduce cytotoxicity	[55]
CRANAD-	2018	780	Aβ42	Mouse	Selective degradation aggregation of Aβ under light irradiation	[65]
Ce6	2019	visible light	Aβ40	PC12	Inhibited the aggregation and toxicity of Aβ under dark conditions, enhancement anti-amyloidogenic activity under illumination	[45]
CRANAD	2019, 2021	660	tau	Mice	Photooxidation inhibited tau amyloid seeding activity	[66]
AQ series	2021	467	Aβ40/Aβ42		Excited-state intramolecular hydrogen transfer in photo-sensitizers plays an important role in controlling the pathological factors of AD	[61]

Declaration of competing interest

The authors declare that they have no known competing financial interests or personal relationships that could have appeared to influence the work reported in this paper.

Acknowledgments

This work was financially supported by the Fundamental Research Funds for the Central Universities and the Research Program on the Relationship between Nicotine and Alzheimer's Disease (No. 110201801035(JY-09)).

References

[1] M.P. Mattson, Nature 430 (2004) 631–639.
[2] D. Liu, D. Fu, L. Zhang, et al., Chin. Chem. Lett. 32 (2021) 1066–1070.
[3] C. Haass, B.D. Strooper, Science 286 (1999) 916–919.
[4] M. Vaz, S. Silvestre, Eur. J. Pharmacol. 887 (2020) 173554.
[5] G.G. Glenner, C.W. Wong, Biochem. Biophys. Res. Commun. 122 (1984) 1131–1135.
[6] D.J. Selkoe, Nat. Med. 17 (2011) 1060–1065.
[7] J. Hardy, D.J. Selkoe, Science 297 (2002) 353–356.
[8] R.E. Tanzi, R.D. Moir, S.L. Wagneret, Neuron 43 (2004) 605–608.
[9] D.J. Selkoe, J. Hardy, EMBO Mol. Med. 8 (2016) 595–608.
[10] C. Haass, D.J. Selkoe, Nat. Rev. Mol. Cell Biol. 8 (2007) 101–112.
[11] S.I. Yoo, M. Yang, J.R. Brender, et al., Angew. Chem. Int. Ed. 50 (2011) 5110–5115.
[12] I.W. Hamley, Chem. Rev. 112 (2012) 5147–5192.
[13] P.E. Cramer, J.R. Cirrito, D.W. Wesson, et al., Science 335 (2012) 1503–1506.
[14] A.R. Ladiwala, J.S. Dordick, P.M. Tessier, J. Biol. Chem. 286 (2011) 3209–3218.
[15] R. Mishra, B. Bulic, D. Sellin, et al., Angew. Chem. Int. Ed. 47 (2008) 4679–4682.
[16] S.S. Hindo, A.M. Mancino, J.J. Braymer, et al., J. Am. Chem. Soc. 131 (2009) 16663–16665.
[17] E.D. Roberson, L. Mucke, Science 314 (2006) 781–784.
[18] K. Ono, K. Hasegawa, H. Naiki, et al., J. Neurosci. Res. 75 (2004) 742–750.
[19] Q.I. Churches, J. Caine, K. Cavanagh, et al., Bioorg. Med. Chem. 24 (2014) 3108–3112.
[20] Á. Juarranz, P. Jaén, F. Sanz-Rodríguez, et al., Clin. Transl. Oncol. 10 (2008) 148–154.
[21] J.P. Celli, B.Q. Spring, I. Rizvi, et al., Chem. Rev. 110 (2010) 2795–2838.
[22] N. Jiang, Z. Zhou, W. Xiong, et al., Chin. Chem. Lett. 32 (2021) 3948–3953.
[23] X. Hu, S. Wang, Q. Luo, et al., Chin. Chem. Lett. 32 (2021) 2287–2291.
[24] Y. Xu, W. Tuo, Y. Sun, et al., Angew. Chem. Int. Ed. 61 (2022) e202110048.
[25] C. Li, Y. Xu, Y. Sun, et al., Chem. Sci. 13 (2022) 6541–6549.
[26] D.W. Felsher, Nat. Rev. Cancer 3 (2003) 375–380.
[27] K. Li, M. Lu, X. Xia, et al., Chin. Chem. Lett. 32 (2021) 1010–1016.
[28] D. Jia, X. Ma, Y. Lu, et al., Chin. Chem. Lett. 32 (2021) 162–167.
[29] Y. Fan, C. Li, Y. Sun, et al., Small 18 (2022) 2201625.
[30] Y. Xu, C. Li, Y. Sun, et al., Nat. Commun. 13 (2022) 2009.
[31] X. Li, B.D. Zheng, X.H. Peng, et al., Coord. Chem. Rev. 379 (2019) 147–160.
[32] C. Wu, Q. Liu, Y. Wang, et al., Chin. Chem. Lett. 32 (2021) 2400–2404.
[33] S. Chen, Y. Liu, R. Liang, et al., Chin. Chem. Lett. 32 (2021) 3903–3906.
[34] B.I. Lee, Y.J. Chung, C.B. Park, Biomaterials 190-191 (2019) 121–132.
[35] W. Liu, X. Dong, Y. Liu, et al., Acta Biomater. 123 (2021) 93–109.
[36] J. Shi, L. Wang, Z. Zhang, et al., Biomaterials 35 (2014) 5771–5784.
[37] B.I. Lee, Y.J. Chung, C.B. Park, et al., Biomaterials 190-191 (2019) 121–132.
[38] J.E. Kim, M. Lee, Biochem. Biophys. Res. Commun. 303 (2003) 576–579.
[39] Y. Ishida, S. Tanimoto, D. Takahashi, et al., Medchemcomm 1 (2010) 212–215.
[40] Y. Ishida, K.Oka T.Fujii, et al., Chem. Asian J. 6 (2011) 2312–2315.
[41] M.A. Rajora, J.W.H. Lou, G. Zheng, et al., Chem. Soc. Rev. 46 (2017) 6433–6469.
[42] M. Masuda, N. Suzuki, S. Taniguchi, et al., Biochemistry 45 (2006) 6085–6094.
[43] A. Hirabayashi, Y. Shindo, K. Oka, et al., Chem. Commun. 50 (2014) 9543–9546.
[44] B.I. Lee, S. Lee, Y.S. Suh, et al., Angew. Chem. Int. Ed. 54 (2015) 11472–11476.
[45] G. Leshem, M. Richman, E. Lisniansky, et al., Chem. Sci. 10 (2019) 208–217.
[46] H. Abrahamse, M.R. Hamblin, Biochem. J. 473 (2016) 347–364.
[47] D. Ozawa, H. Yagi, T. Ban, et al., J. Biol. Chem. 284 (2009) 1009–1017.
[48] P.J. Bjorkman, M.A. Saper, B. Samraoui, et al., Nature 329 (1987) 506–512.
[49] A. Taniguchi, D. Sasaki, A. Shiohara, et al., Angew. Chem. Int. Ed. 53 (2014) 1382–1385.
[50] R. Cibulka, R. Vasold, B. Konig, et al., Chemistry 10 (2004) 6224–6231.
[51] H. LeVine, Meth. Enzymo. 309 (1999) 274–284.
[52] J.S. Lee, B.I. Lee, C.B. Park, Biomaterials 38 (2015) 43–49.
[53] M.R. Mangione, A.P. Piccionello, C. Marino, et al., RSC Adv. 5 (2015) 16540–16548.
[54] B.I. Lee, Y.S. Suh, Y.J. Chung, et al., Sci. Rep. 7 (2017) 7523.
[55] B.I. Lee, Y.S. Suh, et al., Sci. Rep. 7 (2017) 7523.
[56] J.P. Tardivo, A. Del Giglio, et al., Photodiagn. Photodyn. 2 (2005) 175–191.
[57] M. Frank, J. Ahrens, I. Bejenke, et al., J. Am. Chem. Soc. 138 (2016) 8279–8287.
[58] W. Lee, S. Jung, M. Kim, et al., J. Am. Chem. Soc. 143 (2021) 3003–3012.
[59] S.Y. Reece, M.R. Seyedsayamdost, J. Stubbe, et al., J. Am. Chem. Soc. 129 (2007) 8500–8509.
[60] D. Ou Horng, S. Phan, J.D. Thomas, et al., Science 357 (2017) eaag0025.
[61] M. Hong, M. Kim, M.H. Lim, et al., JACS Au 2 (2022) 2001–2012.
[62] W. Ni, W. Chen, Y. Lu, et al., Cancer Med. 7 (2018) 3820–3833.
[63] A. Kamkaew, S.H. Lim, K. Burgess, et al., Chem. Soc. Rev. 42 (2013) 77–88.
[64] C. Ran, X. Xu, S.B. Raymond, et al., J. Am. Chem. Soc. 131 (2009) 15257–15261.
[65] J. Ni, A. Taniguchi, S. Ozawa, et al., Chem 4 (2018) 807–820.
[66] T. Suzuki, Y. Hori, T. Sawazaki, et al., Chem. Commun. 55 (2019) 6165–6168.
[67] S. Ozawa, Y. Hori, Y. Shimizu, et al., Brain 144 (2021) 1884–1897.
[68] K.P. Kepp, Chem. Rev. 112 (2012) 5193–5239.
[69] H. Zeng, Y. Qi, Z. Zhang, et al., Chin. Chem. Lett. 32 (2021) 1857–1868.
[70] Q. Yu, X. Wang, L. Nie, Chin. Chem. Lett. 32 (2021) 1879–1887.
[71] J. Nasica-Labouze, P.H. Nguyen, F. Sterpone, et al., Chem. Rev. 115 (2015) 3518–3563.
[72] L. Sun, Y. Lei, Y. Wang, D. Liu, Chin. Chem. Lett. 33 (2022) 1946–1950.
[73] X. Liu, Y. Qin, J. Zhu, et al., Chin. Chem. Lett. 32 (2021) 1537–1540.
[74] Y. Wang, Q. Zhou, X. He, et al., Chin. Chem. Lett. 33 (2022) 1613–1618.
[75] B. Huang, X. Liu, G. Yang, et al., CCS Chem. 4 (2022) 2090–2101.